Probing half β_y^* optics in the Accelerator Test Facility 2

M. Patecki,* D. Bett, E. Marin, F. Plassard, and R. Tomás
European Organization for Nuclear Research (CERN), CH-1211 Geneva 23, Switzerland

K. Kubo, S. Kuroda, T. Naito, T. Okugi, T. Tauchi, and N. Terunuma
High Energy Accelerator Research Organization (KEK), Tsukuba, Ibaraki 305-0801, Japan, and School of High Energy Accelerator Science, (SOKENDAI), Tsukuba, Ibaraki 305-0801, Japan
(Received 29 July 2016; published 5 October 2016)

A nanometer beam size at the interaction point (IP) is required for future linear colliders to achieve the desired rate of particle collisions. KEK Accelerator Test Facility 2 (ATF2), a scaled down implementation of the linear collider beam delivery system, serves for demonstrating the feasibility of the final focus system (FFS). An unprecedented low vertical beam size at the IP of about 40 nm has been already measured in ATF2 using the optics with a nominal β_y^*. In our study we decrease the β_y^* value in order to investigate the performance of more chromatic optics and to study the limits of beam focusing at the IP. Stronger beam focusing amplifies the aberrations from the final focus imperfections which cause an increase of the beam size at the IP. Simulations show that the multipolar errors and final doublet fringe fields spoil the IP beam sizes for ultralow β_y^* optics but can be mitigated either by increasing the value of the horizontal β^* or installing a pair of octupole magnets. We report on our first experimental steps towards the ultralow β_y^* in ATF2. New methods for the beam diagnostics at the IP were developed in order to precisely set the desired optics. β_y^* value was half the nominal value. The beam tuning was performed and the measured beam size is compared with the simulation results.

DOI: 10.1103/PhysRevAccelBeams.19.101001

I. INTRODUCTION

In the future linear collider (CLIC [1], ILC [2]) the high collision rate will be achieved by colliding the beams demagnified to nanometer size at the interaction point (IP). A pair of strong quadrupole magnets, called the final doublet (FD), are used to focus the beam at the IP. Chromatic effects associated with the FD quadrupoles mean that off-momentum particles are not focused exactly at the focal point, leading to larger spot sizes at the IP. A novel design of the final focus system with a local compensation of chromatic aberrations [3] is being tested in ATF2 [4,5]. It has already been demonstrated that the IP vertical beam size in ATF2 decreases from some hundreds of nanometers to about 40 nm [6–8] when the chromaticity is corrected. Therefore, the local chromaticity correction scheme is considered as a baseline for ILC and a strong candidate for CLIC. However, for CLIC the expected level of chromaticity is higher by about a factor 5. For this reason, the ultralow β_y^* optics [9–11] are being carried out at ATF2 with the aim of increasing the level of chromaticity. The chromaticity roughly scales as $\zeta_y \sim L^*/\beta_y^*$ (L^* is the last drift before the IP), so it can be increased by decreasing the β_y^* value, initially by a factor 2 to test a halfway moderated step and finally by a factor 4, which brings the chromaticity level close to CLIC (see Table I). In principle, lowering the β_y^* value allows IP beam sizes closer to those of a future linear collider to be reached. However, magnetic imperfections such as multipolar errors [11] and fringe fields [12] may limit the IP beam size. Understanding the trade-offs between lowering β_y^* and increasing aberrations is of critical importance for future linear colliders.

In this study we decrease the β_y^* value from 100 μm (nominal β_y^*) to 50 μm (half β_y^*). The nominal value of β_x^* is 4 mm but in recent ATF2 operation $10\beta_x^* = 40$ mm is used as it better corresponds to the expected strength of the optical aberrations in ILC [8]. The β_x^* values used in our study are 40 mm ($10\beta_x^*$) and 100 mm ($25\beta_x^*$). See Table I for the comparison of main parameters of the considered lattices of CLIC, ILC and ATF2.

A. High order multipole fields and fringe fields of the ATF2 magnets

The increase of the β_y function in the ATF2 final focus region caused by lower β_y^* value is depicted in Fig. 1. The magnetic imperfections are amplified in high β_y regions and may cause an increase in the IP beam size. The impact of carefully measured [13,14] multipolar errors of the ATF2

*Also at Warsaw University of Technology, Pl. Politechniki 1, 00-661 Warsaw, Poland.
mpatecki@cern.ch

TABLE I. Some of the FFS parameters for ATF2, CLIC and ILC.

	$\varepsilon_{y,\text{design}}$ [pm]	$\varepsilon_{y,\text{meas.}}$ [pm]	β_x^* [mm]	β_y^* [μm]	$\sigma_{y,\text{design}}^*$ [nm]	$\sigma_{y,\text{meas.}}^*$ [nm]	L^* [m]	$\zeta_y \sim (L^*/\beta_y^*)$
ILC	0.07	⋯	11	480	5.9	⋯	3.5/4.5	7300/9400
CLIC	0.003	⋯	4	70	1	⋯	3.5	50000
ATF2 nominal	12	⋯	4	100	37	⋯	1	10000
ATF2 nominal, $10\beta_x^*$	12	⋯	40	100	37	(44 ± 3)[a]	1	10000
ATF2 half β_y^*	12	⋯	4	50	30.5, 25[b]	⋯	1	20000
ATF2 half β_y^*, $10\beta_x^*$	12	(7.7 ± 0.3)[c]	40	50	26	(58 ± 5)[c]	1	20000
ATF2 half β_y^*, $25\beta_x^*$	12	(7.7 ± 0.3)[c]	100	50	25	(51 ± 6)[c]	1	20000
ATF2 ultralow β_y^*	12	⋯	4	25	27, 20[2]	⋯	1	40000
ATF2 ultralow β_y^*, $10\beta_x^*$	12	⋯	40	25	21	⋯	1	40000

[a]In [7].
[b]Using octupole magnets.
[c]In this paper.

magnets on the IP beam size was reported in [11]. For the ultralow β_y^* optics the multipolar errors cause the IP beam size to increase from 20 to 27 nm, which is not satisfactory. The IP beam size was calculated using the high-order transfer map obtained with the *polymorphic tracking code* [15] and the MAPCLASS [16] code using the methods described in [17].

Another limitation in reaching the target beam size is the magnetic fringe fields of the final doublet quadrupoles, as reported in [12]. For the nominal β_y^* value the impact of fringe fields is negligible but it gets amplified as the β_y function increases for the ultralow β_y^* optics. The quadrupolar fringe fields can be represented as third order kicks [18,19] applied to particles at both ends of the magnets causing the IP beam size to increase.

Both multipolar errors and fringe fields set a limit for the efficiency of beam focusing and require correction. Mitigation methods are described in the next section.

B. Mitigation methods

From Table I one can see that the IP vertical beam size is significantly lower (for half and ultralow β_y^*) when the β_x^* is increased by a factor 10. This is due to the lower β function in the FFS. However, in such a case the horizontal beam size increases by a factor $\sqrt{10}$. For linear colliders increasing the horizontal IP beam size to reduce aberrations in the vertical plane is not a favorable solution as it may reduce luminosity.

Another mitigation method considered is the installation of two octupole magnets in the ATF2 beam line. Some aberrations are corrected with the use of sextupole magnets, but detailed analysis of the multipole components at ATF2 [11] revealed the strong third order contribution coming from the QD0FF magnet (last quadrupole before the IP). Also the FD fringe fields give mainly third order kicks which justifies the use of octupole magnets. The installation of two octupole magnets is planned, one in a dispersive and the other in a nondispersive location, with a phase advance of 180° between them. The proposed locations for the octupole magnets are: OCT1FF between QD2AFF and SK1FF and OCT2FF between QD6FF and SK3FF. The technical design [20,21] of the magnets was done at CERN. The octupole magnets are already assembled and their properties are being tested at CERN. Their installation in ATF2 is expected for autumn 2016. The simulated vertical beam size decreases from 27 to 20 nm when the octupoles are added to the beam line.

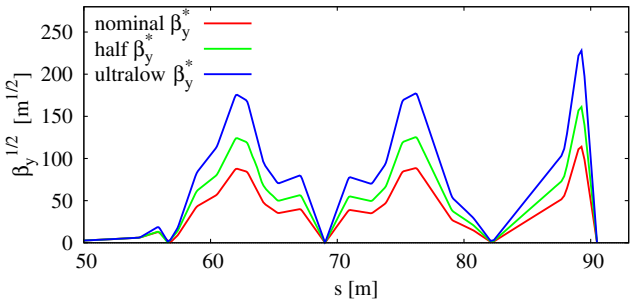

FIG. 1. β_y function along the ATF2 beam line in the case of nominal β_y^*, half β_y^* and ultralow β_y^* optics.

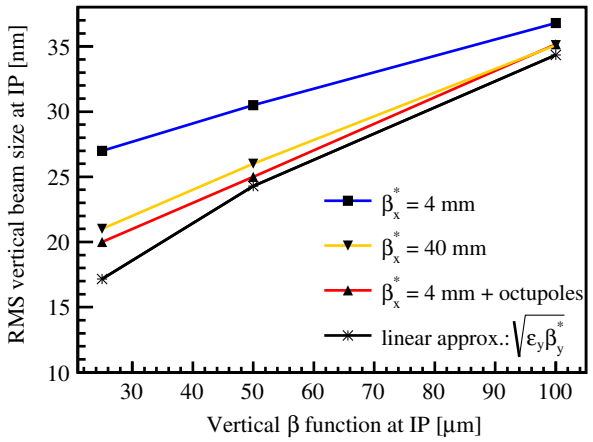

FIG. 2. Expected vertical beam size in ATF2 for three considered β_y^* values and proposed mitigation methods.

A comparison of expected vertical beam sizes at the IP for the considered mitigation methods is presented in Fig. 2.

II. FIRST EXPERIMENTS WITH THE HALF β_y^* OPTICS

Experimental studies towards the ultralow β_y^* have been performed at ATF2 since December 2014. We started with the half β_y^*, $10\beta_x^*$ optics (see Table I). The optics matching and diagnostics in low β_y^* conditions are also more challenging and the development of special procedures was needed. In the next sections we report on the beam operation in half β_y^*, $10\beta_x^*$ optics performed in the last week of February 2016.

A. Matching the beam parameters at the IP

Six quadrupole magnets located at the entrance of the final focus line are used to match the beam parameters at the IP. The required quadrupole strengths are calculated using the machine model. However, for every beam operation the initial beam parameters at the extraction from the damping ring are slightly different which then affects the matching solution. Therefore, the precise matching of the beam parameters at the IP is done in two iterations. In the first iteration it is assumed that the initial beam parameters are exactly the same as in the model and the calculated solution is applied to the machine. Then the beam parameters at the IP are measured. If the measured values do not meet the matching target, the matching solution is recalculated taking into account the observed discrepancy. The procedures for precise measurement of the beam parameters at the IP are described in the next two sections.

B. Beam diagnostics at the IP

Quadrupole scanning is a widely used method (also in ATF2 [22]) for measuring the transverse beam parameters. Since we are interested in the beam parameters at the IP, the FD quadrupoles strength is varied and both horizontal and vertical beam sizes are measured using the IP wire scanner. An increase of the transverse beam size due to the beam waist shift is defined by the beam divergence, so the beam parameters can be resolved by fitting Eq. (1) to the square of the measured beam size $\sigma_{x,y}^2$, where $\varepsilon_{x,y}$ stands for the transverse emittance, $\beta_{x,y}^*$ for the IP β value and $\Delta f_{x,y}$ for the longitudinal distance between the wire position and actual beam waist position:

$$\sigma_{x,y}^2 = \varepsilon_{x,y}\beta_{x,y}^* + \frac{\varepsilon_{x,y}}{\beta_{x,y}^*}(\Delta f_{x,y})^2. \quad (1)$$

Similarly to the method described in [22] the measured beam size has to be corrected for residual dispersion at the IP and for the geometric properties of the wire, as given in Eq. (2):

$$\sigma_{x,y}^2 = \sigma_{x,y,\text{measured}}^2 - \left(\frac{\sigma_E}{E}\right)^2 D_{x,y}^2 - \left(\frac{d}{4}\right)^2, \quad (2)$$

where $\frac{\sigma_E}{E}$ is the relative energy spread (equal to 0.0006 for low beam intensity of $10^9 e^-$/bunch) and $d = 5$ μm is the carbon wire diameter.

The minimum measurable beam size with the wire scanner is about half of the wire diameter, which is not an obstacle for horizontal beam size measurement (between 6 and 10 μm is the usual value in recent operation). However, the vertical beam size is expected to be smaller than 1 μm even for the beginning of the operation and it cannot be precisely measured when the beam waist is at the wire location. Instead, the beam waist is shifted out of the wire location so that the beam divergence can be resolved using Eq. (3):

$$\sigma_y^2 \approx \frac{\varepsilon_y}{\beta_y^*}(\Delta f_y)^2. \quad (3)$$

An example of vertical beam divergence evaluation is presented in Fig. 3.

Knowledge of β_y^* is necessary for judging if the desired optics were correctly implemented. For the horizontal plane both emittance and β^* can be resolved but in the vertical plane the β^* value can be calculated only if the vertical emittance is known, e.g. measured upstream. In the last week of February 2016 operation the vertical emittance was measured in the damping ring (DR) using the x-ray synchrotron radiation (XSR) monitor [23] and in the extraction line (EXT) using the optical transition radiation monitors (mOTR) [24]. Table II contains the measured values of the emittance and corresponding values of β_y^*. The large difference in the vertical emittance might imply that the mOTR measurement is biased with a large unknown systematic error and cannot provide a reliable estimate of the emittance. On the other hand the XSR measurement cannot be used either as some emittance growth is expected after beam extraction from the damping ring [25]. A new

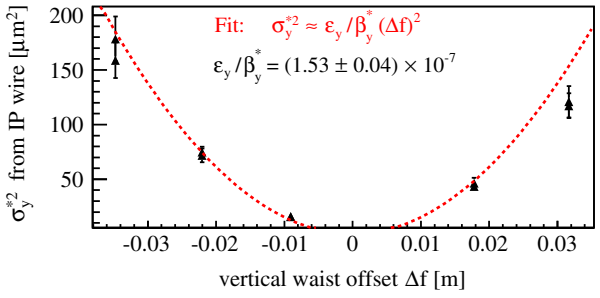

FIG. 3. Example of QD0FF scan for vertical beam parameters evaluation at the IP from the last week of February 2016 operation. Lower cut for the beam size measurement was set to 3 μm. Only the ratio ε_y/β_y^* can be resolved. The effects of dispersion and wire properties are subtracted. Change of the β_y^* value for the maximum waist offset is less than 5%.

TABLE II. β_y^* evaluation based on two emittance measurements and a QD0FF scan performed in the last week of February 2016 operation. The matching target was $\beta_y^* = 50$ μm.

	ε_y [pm]	β_y^* [μm]
DR (XSR)	4.4 ± 0.4	29.0 ± 3.0
EXT (mOTR)	15.3 ± 1.5	100.0 ± 10.1

method for IP vertical emittance evaluation was therefore introduced and is described in the next section.

C. New method for IP vertical emittance measurement

As mentioned, the quadrupole scan method cannot be applied in the vertical plane to resolve both the emittance and β^* value since the vertical beam size at the waist is too small to be measured by the wire scanner. This obstacle can be overcome by using the Shintake monitor [26,27] located at the IP for measuring the vertical beam size. It is an interference monitor where two laser beams cross in the plane transverse to the electron beam in order to form a vertical interference pattern, see Fig. 4. The beam size is inferred from the modulation of the resulting Compton scattered photon signal detected by a downstream photon detector, see Eq. (4):

$$M = C|\cos\theta| \exp\left[-2(k_y\sigma_y)^2\right],$$
$$k_y = \pi/d, \qquad d = \frac{\lambda}{2\sin(\theta/2)}, \tag{4}$$

where C is the modulation reduction factor which represents the overall systematic effect causing a decrease of the observed modulation due to the monitor imperfections, θ is the crossing angle and $\lambda = 532$ nm is the laser wavelength. Three laser crossing angle modes (2–8 degree, 30 degree, 174 degree) extend the dynamic range from 5 μm to 20 nm.

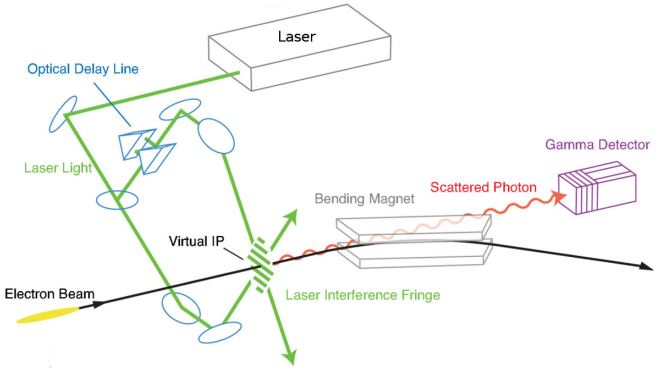

FIG. 4. Shintake monitor schematic design. The electron beam interacts with a transverse interference pattern generated by two crossing laser beams. The number of scattered photons varies with the fringe size and the particle beam size [6].

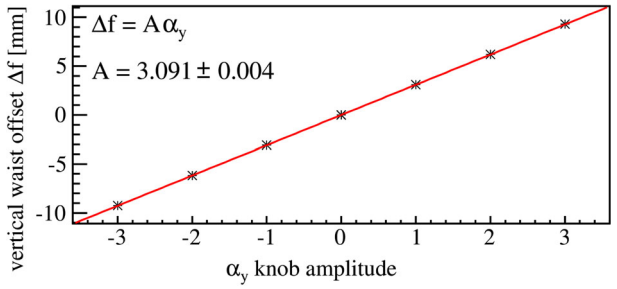

FIG. 5. The relation between α_y knob amplitude and beam waist offset derived from the simulations. A is the proportionality coefficient.

The 30 degree mode with a dynamic range of 85 to 340 nm is the most precise and its systematic errors can be accurately measured, so this mode should be chosen to perform the scan. Such a narrow dynamic range of the beam size measurement in 30 degree mode requires very fine, well controlled beam waist shifts of less than 5 mm. This cannot be achieved by varying the strength of the QD0FF magnet, so the vertical beam waist position knob [28] (the so-called α_y knob) is used instead. This knob makes use of deliberate horizontal movements of the FFS normal sextupole magnets and it modifies the vertical beam waist position without changing the other beam parameters [28]. The relation between α_y knob amplitude and beam waist offset is depicted in Fig. 5.

In the last week of February 2016 operation the optics were rematched with target β^* values of $\beta_x^* = 40$ mm and $\beta_y^* = 2.5$ mm (β_y^* being 25 times larger than nominal) in order to increase the vertical beam size at the IP such that it can be measured with the 30 degree mode of the Shintake monitor. The α_y scan was then performed and the measured data were fitted (see Fig. 6) with the formula [Eq. (5)] coming from combining Eq. (1) with Eq. (4):

$$M = C_{30}\cos(30°)\exp\left[-2k_y^2\left(\varepsilon_y\beta_y^* + \frac{\varepsilon_y}{\beta_y^*}(A\Delta\alpha_y)^2\right)\right]. \tag{5}$$

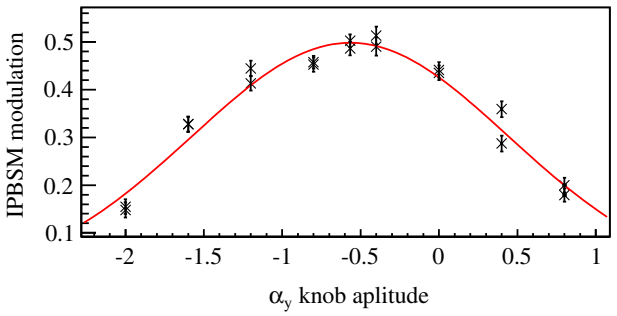

FIG. 6. Measured modulation during the α_y scan to resolve the vertical emittance at the IP and the β_y^* value using the Shintake monitor in 30 degree mode.

The modulation reduction factor in 30 degree mode (C_{30}) was estimated in the same beam operation in the following way. The optics was rematched with target β^* values of $\beta_x^* = 40$ mm and $\beta_y^* = 50$ μm in order to decrease the vertical beam size such that it can be measured both in 30 and 174 degree mode. The modulation was then measured by taking ten consecutive Shintake monitor scans, first in 174 degree mode: $M_{174,\text{meas.}} = 0.374 \pm 0.016$ (stat); and immediately after in 30 degree mode: $M_{30,\text{meas.}} = 0.709 \pm 0.016$ (stat). Using the modulation in 174 degree mode ($M_{174,\text{meas.}}$) the corresponding beam size (σ_{174}) was calculated according to

$$\sigma_{174} = \frac{1}{2k_y}\sqrt{2\ln\left(\frac{C_{174}|\cos(174°)|}{M_{174,\text{meas.}}}\right)}, \tag{6}$$

where C_{174} is the modulation reduction factor in 174 degree mode. The uncertainty of the beam size evaluation is given by

$$\Delta\sigma_{174} = \frac{1}{4k_y^2\sigma_{174}}\sqrt{\left(\frac{\Delta M_{174,\text{meas.}}}{M_{174,\text{meas.}}}\right)^2 + \left(\frac{\Delta C_{174}}{C_{174}}\right)^2}, \tag{7}$$

where $\Delta M_{174,\text{meas.}}$ and ΔC_{174} stand for the uncertainties of $M_{174,\text{meas.}}$ and C_{174} respectively. The modulation reduction factor of the Shintake monitor in 174 degree mode (C_{174}) cannot be directly measured and its estimation requires a complex off-line analysis. An attempt at estimating C_{174} is described in the Ph.D. thesis of Yan [27], but in our study we assume $C_{174} = 1^{+0.0}_{-0.1}$ which allows us to calculate the upper limit of the measured beam size and accounts for possible hardware imperfections of the Shintake monitor causing a decrease of the measured modulation. Such an approach is applied to all beam size calculations (in 174 degree mode) shown in this paper.

The expected modulation in 30 degree mode was calculated in the following way:

$$\begin{aligned} M_{30,\text{exp}}(\sigma_{174}) &= \cos(30°)\exp\left[-2(k_y\sigma_{174})^2\right] \\ &= 0.81 \pm 0.01 \end{aligned} \tag{8}$$

and compared with a measured value ($M_{30,\text{meas.}}$). The ratio of these two is the modulation reduction factor in 30 degree mode:

$$C_{30} = \frac{M_{30,\text{meas.}}}{M_{30,\text{exp}}(\sigma_{174})} = 0.87 \pm 0.02. \tag{9}$$

The vertical beam parameters at the IP, namely vertical emittance and β_y^* value, were resolved from fitting α_y scan data with the formula given in Eq. (5), as presented in Fig. 6. In our case the results are $\varepsilon_y = 7.7 \pm 0.3$ pm and $\beta_y^* = 2.81 \pm 0.12$ mm (matching target was $\beta_y^* = 2.5$ mm).

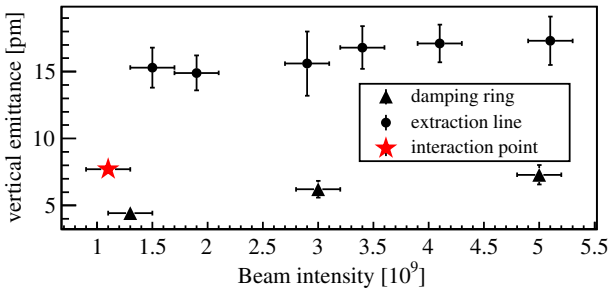

FIG. 7. Comparison of measured vertical emittance at three locations using different methods versus beam intensity. Emittance at the IP was measured only for one beam intensity but this study is ongoing.

The vertical emittance measured with this method is compared to the XSR measurements in the DR and mOTR measurements in the EXT line during the same week of operation; see Fig. 7. A vertical emittance growth between the DR and IP nearly by a factor 2 is observed. These data also confirm that there might be some issues with the mOTR system.

This vertical emittance was then used to verify if the half β_y^* optics were correctly applied. The vertical beam divergence squared measured by scanning QD0FF (Fig. 3) was $\varepsilon_y/\beta_y^* = (1.53 \pm 0.04) \times 10^{-7}$ which gives $\beta_y^* = 50 \pm 2$ μm. The β_y^* value agrees with the matching target (50 μm) proving that the desired optics were correctly applied to the machine.

D. Beam tuning and IP beam size measurements in half β_y^* optics

Beam tuning is the process of adjusting the machine parameters to bring the IP beam size as close as possible to the design value. It consists of matching the dispersion and β function, steering the orbit, correcting the coupling and minimizing the residual aberrations. A detailed description of beam tuning procedures used at ATF2 together with definitions of the knobs can be found in [5,28]. The IP vertical beam size measured with the Shintake monitor in 174 degree mode is used as a figure of merit for the tuning. After the initial tuning, the vertical beam size is dominated by the linear aberrations of beam waist longitudinal position shift, vertical dispersion and $x'y$ coupling. For each of these aberrations there is a dedicated knob, respectively Ay, Ey and C_2, constructed to be orthogonal by using deliberate horizontal and vertical displacements of the normal sextupole magnets. The nonlinear beam aberrations are corrected with the second order tuning knobs ($Y22$, $Y24$, $Y26$, $Y44$, $Y46$, $Y66$) by changing the strength of the normal and skew sextupole magnets. The digits relate to coordinate indexes (x, x', y, y', ct, δ) of the corresponding correlation, e.g.:

$$Y26 = \frac{\langle (y - \langle y\rangle)(x' - \langle x'\rangle)(\delta - \langle\delta\rangle)\rangle}{\sqrt{\langle (x' - \langle x'\rangle)^2(\delta - \langle\delta\rangle)^2\rangle}} \tag{10}$$

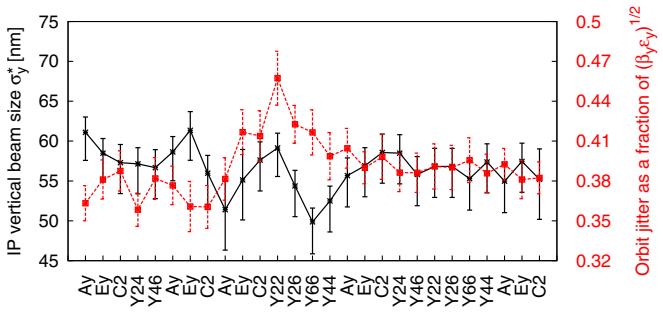

FIG. 8. IP vertical beam size (black) and the orbit jitter (red) versus the beam tuning in half β_y^*, $10\beta_x^*$ optics. Points representing the beam size correspond to the optimum knob setting and error bars account for the uncertainty of finding the optimum knob setting by fitting the knob scan data (as in Fig. 6) and for the systematic error of the Shintake monitor as described in Sec. II C.

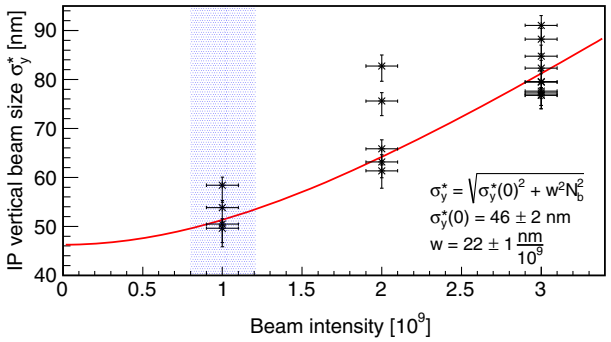

FIG. 9. Intensity dependence of IP vertical beam size for half β_y^*, $10\beta_x^*$ optics. Black points stand for the measured beam size, red curve for the fit according to Eq. (11) and blue band for the bunch intensity restriction of the tuning and final beam size measurement.

is the aberration coming from the correlation between vertical position (y), horizontal angle (x') and relative momentum deviation (δ) of the electrons at the IP.

In the last week of February 2016 operation the full tuning in half β_y^*, $10\beta_x^*$ optics was done; the beam size improvement versus the applied knob is depicted in Fig. 8. One can see that the tuning efficiency is low which probably means that the initial knob settings were close to optimum and any possible further beam size improvement was spoiled by other sources of IP beam size growth. The IP beam size increase coincides with large orbit position jitter in the final focus line (also shown in Fig. 8) suggesting that the orbit position jitter in the final focus line affects the IP beam size and tuning efficiency. Other possible reasons for low tuning efficiency are Shintake monitor fluctuations, beam intensity fluctuations and wakefields. Shintake monitor fluctuations are included in the uncertainty of the beam size measurement (an error of the modulation reduction factor as described in Sec. II C). Beam intensity fluctuations increase the errors of the Shintake monitor and contribute to the wakefield effect on the beam size. The effect of beam intensity fluctuations are minimized by selecting only the bunches with an intensity of $(0.8, 1.2) \times 10^9 e^-$ to be measured by the Shintake monitor. We express the wakefield contribution to the IP vertical beam size as

$$\sigma_y^* = \sqrt{\sigma_y^*(0)^2 + w^2 N_b^2}, \tag{11}$$

where $\sigma_y^*(0)$ is the zero-intensity (no wakefield effect) IP vertical beam size, w the wakefield contribution, and N_b the bunch intensity [5]. The contribution of wakefields on the IP vertical beam size for half β_y^*, $10\beta_x^*$ optics was investigated by measuring the IP vertical beam size for three bunch intensities: $1 \times 10^9 e^-$, $2 \times 10^9 e^-$ and $3 \times 10^9 e^-$, see Fig. 9. The obtained value of $w = 22 \pm 1 \frac{nm}{10^9 e^-}$ corresponds well with the simulations described in [8]. In that study the known wake potentials of beam line cavities, flanges and bellows were combined with the beam orbit jitter in the final focus line in order to investigate their impact on the IP beam sizes. For the beam orbit jitter of 40% of the beam size and half β_y^*, $10\beta_x^*$ optics the estimated value of w is $18 \frac{nm}{10^9 e^-}$ [8]. Small discrepancy with respect to the measured value suggests that some wakefield sources were not implemented in the simulation. The wakefield contribution for bunch intensity in the range $(0.8, 1.2) \times 10^9 e^-$ does not explain the discrepancy between the measured and expected IP vertical beam sizes. Moreover, in consequence of reducing the bunch intensity the resolution of the beam position monitors (BPM) is worsened and the signal-to-noise ratio of the Shintake monitor is increased. For the nominal β_y^* the IP vertical beam size increase due to wakefields combined with the final focus line beam jitter of 40% of the beam size is $15 \frac{nm}{10^9 e^-}$ [8] showing that the wakefield contribution is enhanced when the β_y^* value is lowered. More systematic measurements of the wakefield contribution to the IP vertical beam size for different optics is foreseen for autumn 2016 operation in the ATF2. After the tuning, the final beam size was measured by taking ten consecutive beam size measurements; the result is given in Table III.

In the next step, the horizontal β_x^* was relaxed to $25\beta_x^*$. The beam tuning was again performed (see Fig. 10) and the final beam size was measured as in the previous case (see Table III). For these optics we have observed an increased tuning efficiency and the measured IP vertical beam size is

TABLE III. Measured IP vertical beam size after the tuning for half β_y^*, $10\beta_x^*$ optics and half β_y^*, $25\beta_x^*$ optics compared with the design values assuming the measured vertical emittance.

Optics	$\sigma^*_{y,\text{meas.}}$ [nm]	$\sigma^*_{y,\text{design}}$ [nm] (for $\varepsilon_y = 7.7$ pm)
Half β_y^*, $10\beta_x^*$	58^{+4}_{-5}	21
Half β_y^*, $25\beta_x^*$	51^{+5}_{-6}	20

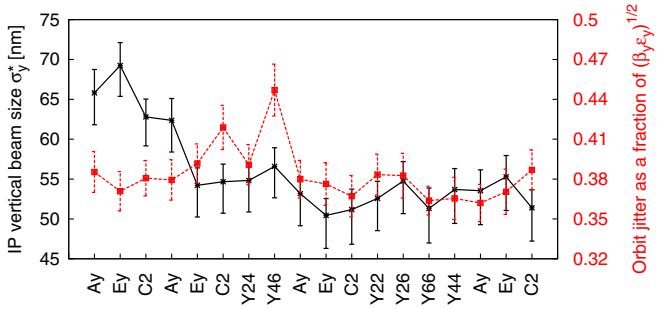

FIG. 10. IP vertical beam size (black) and the orbit jitter (red) versus the beam tuning in half β_y^*, $25\beta_x^*$ optics. Points representing the beam size correspond to the optimum knob setting and error bars account for the uncertainty of finding the optimum knob setting by fitting the knob scan data (as in Fig. 6) and for the systematic error of Shintake monitor as described in Sec. II C.

lower by 12% with respect to the IP vertical beam size for half β_y^*, $10\beta_x^*$ optics. Relaxing the horizontal optics reduces the sensitivity to nonlinear aberrations but does not help with the other beam size growth sources. Moreover, for a larger β_x^* value the larger IP horizontal beam size more strongly affects the IP vertical beam size in the case of xy coupling.

E. Beam tuning simulations

Tuning simulations using the MAD-X [29] model of the ATF2 beam line were performed in order to understand the measured beam sizes (see Table III). The errors applied to the magnets in the ATF2 model concern the measured multipolar components and realistic random errors on the transverse alignment, roll angle and strength of the ATF2 magnets. The usually assumed values of errors [28] are 100 μm for transverse alignment, 200 μrad for roll angle and 0.1% for strength. In our simulations we consider also misalignments larger by 50% and 100% and multipolar errors larger by factors of 3 and 5. We performed the simulations in two cases in terms of the orbit correction: with orbit correction given by the MAD-X CORRECT [29] command, which uses the beam line BPMs and correctors, and without any simulated orbit correction. The BPMs used for the orbit correction are centered with the adjacent magnets with additional position error of 10 μm which accounts for the mounting precision and readout errors. The orbit correction is applied only once just after misaligning the magnets as the machine drifts are not simulated. The knobs used for the tuning simulations are defined in the same way as for the actual machine and applied in the same order and number.

The IP beam size is calculated from the electron distribution at the IP convoluted with the Shintake monitor fringe pattern. Additionally, the beam size growth coming from the effect of wakefields combined with the beam angular jitter at the IP and the Shintake monitor performance is included by adding in quadrature the corresponding random errors of 18 ± 4 nm (Gaussian distribution) [8] and ± 8 nm (uniform distribution) [28] respectively. One hundred seeds were used for every considered machine setup. The results are summarized in Table IV where IP vertical beam size is represented by the mean value over all seeds ($\sigma_{y,\mathrm{sim}}^*$) and the spread of the results is given by the standard deviation of the beam size data.

F. Discussion of the results

In the case with the orbit correction included in the simulations the obtained beam sizes (last two columns of Table IV) are always lower than in the experiment. If the ATF2 orbit correction was as good as in the simulations, the multipolar errors would require a considerably larger factor which would be unrealistic. This suggests that the orbit correction applied at ATF2 might be not very efficient and its improvement could help to reach low beam sizes. In the ATF2 the orbit correction is done manually, first (at the beginning of beam operation) to minimise the beam offset at the BPMs and later during the beam tuning individual correctors are scanned to minimize the IP beam size.

TABLE IV. Mean and standard deviation of the IP vertical beam size obtained from the tuning simulations for half β_y^*, $10\beta_x^*$ (10×0.5) and half β_y^*, $25\beta_x^*$ (25×0.5) optics for various sets of machine errors.

	Misalignments				$\sigma_{y,\mathrm{sim}}^*$ [nm] *w/o* orbit corr.		$\sigma_{y,\mathrm{sim}}^*$ [nm] *w/* orbit corr.	
Case	Δx [μm]	Δy [μm]	$\Delta\theta$ [μrad]	Multipolar errors	half β_y^*, $10\beta_x^*$	half β_y^*, $25\beta_x^*$	half β_y^*, $10\beta_x^*$	half β_y^*, $25\beta_x^*$
Nominal err.	100	100	200	x1	39 ± 10	38 ± 7	32 ± 3	32 ± 3
Misalignments x1.5	150	150	300	x1	52 ± 22	49 ± 13	36 ± 8	35 ± 5
Misalignments x2.0	200	200	400	x1	67 ± 30	62 ± 20	39 ± 10	40 ± 8
Multipolar err. x3	100	100	200	x3	44 ± 10	46 ± 10	38 ± 6	37 ± 5
Multipolar err. x5	100	100	200	x5	61 ± 14	54 ± 11	45 ± 8	44 ± 7
Misalignments x1.5, multipolar err. x3	150	150	300	x3	62 ± 24	55 ± 16	42 ± 7	42 ± 8
Misalignments x2.0, multipolar err. x5	200	200	400	x5	85 ± 33	74 ± 22	54 ± 12	55 ± 11
Experiment	...	...	...	...	...	...	(58^{+4}_{-5})[a]	(51^{+5}_{-6})[a]

[a]Orbit correction in the experiment is different than in the simulation.

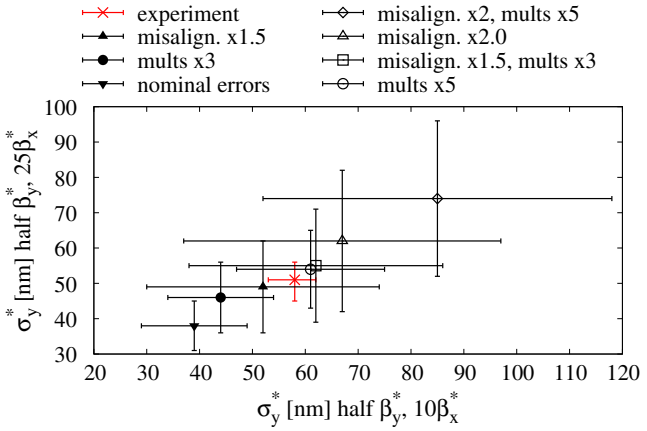

FIG. 11. The IP beam sizes measured in ATF2 (red) and obtained with simulations without the orbit correction (black) for half β_y^*, $10\beta_x^*$ and half β_y^*, $25\beta_x^*$ optics.

Performance of the initial orbit steering depends on the beam line elements alignment and BPMs calibration. The mechanical alignment of the final focus system magnets was done in October 2015 and the BPMs calibration was done in December 2015. The initial steering degrades with time due to machine drifts and jitters. Some sources of machine drifts and jitters are related to the water cooling system and air temperature in the damping ring [8]. In the ATF2 there is also an orbit feedback system that keeps the constant beam position at the selected BPM. However, this system is slow and sensitive to the optics match constraints and its performance is spoiled when the beam is operated at low intensity.

The simulated beam sizes better correspond to the experiment when the orbit correction is not applied (see Fig. 11) which may reflect limitations of the ATF2 orbit correction methods. For the nominal machine errors the simulated beam sizes are 33% lower than in reality for half β_y^*, $10\beta_x^*$ optics and 25% lower for half β_y^*, $25\beta_x^*$ optics. As the machine errors increase, the simulated beam sizes get closer to the measured values, especially for the following cases: misalignments x1.5; multipolar err. x5; misalignments x1.5, multipolar err. x3 (see Fig. 11). The combined effect of larger magnet misalignments and stronger multipolar errors is a possible explanation of the beam sizes measured in ATF2.

The strong effect of the nonlinear aberrations was observed in the experiment by switching off the skew sextupole magnets. When the skew sextupoles (used for the following nonlinear knobs: $Y22$, $Y26$, $Y44$, $Y66$) were turned off after the tuning, the measured beam sizes increased of about 20 nm for both optics [30,31]. Some of this beam size increase can come from the magnetic feeddown effect due to the horizontal and vertical offsets at the skew sextupoles. However, the beam based alignment of the skew sextupoles was done shortly before these beam operations and the linear knobs correction was usually small after these nonlinear knobs which suggest that most of this beam size increase comes from the nonlinear aberrations that seem to be stronger than anticipated in ATF2. The source of possible larger multipolar errors is unknown since careful magnetic measurements were carried out. We suspect that some additional multipolar fields can be induced due to the crosstalk of the quadrupoles, normal sextupoles and skew sextupoles being very close to each other in the final doublet region. Further experimental tests with and without the octupoles should be carried in the future to shed light on this matter. Moreover, the strong nonlinear aberrations strengthen the role of the octupole magnets, not only for ultralow β_y^* optics, but also for the nominal optics with $1\beta_x^*$.

We identify the main reasons for observing larger beam sizes than expected: insufficient orbit control and sensitivity to machine drifts, contribution of wakefields combined with the beam orbit jitter, larger multipolar fields, larger magnet alignment errors, instrumentation errors and stability (especially Shintake monitor and BPMs). All these factors are strongly related as large orbit offsets can be interpreted as larger misalignments causing a stronger effect due to multipolar errors and stronger wakefields contribution. Addressing these issues is recommended for a future experiment with low β_y^* optics.

III. CONCLUSION

The half β_y^* optics has been studied at ATF2 as a first experimental step towards ultralow β_y^*. The optics control and implementation was achieved by introducing a new method of beam diagnostics at the IP based on precise beam size measurements and fine, well-controlled changes of the vertical beam waist position. The beam sizes measured after two complete tuning sessions were almost a factor 3 larger than the design values (assuming measured vertical emittance). It was observed that the IP beam size increase coincides with large orbit position jitter in the final focus line. On the other hand, the machine operated with the nominal β_y^*, $10\beta_x^*$ optics is close to reach the design performance in terms of IP vertical beam size as was demonstrated in early 2016 ATF2 operation [8]. This suggests that the beam size growth due to machine imperfections for lower β_y^* values is much stronger than expected in the design. The realistic errors applied to the machine model are not sufficient to reproduce the experimental results. Simulation results get closer to the experiment for larger machine errors, especially for the following cases: misalignments x1.5; multipolar err. x5; misalignments x1.5, multipolar err. x3. It is also possible that there are other sources of beam size growth which are not included in the simulations.

Simulations also show that an accurate orbit correction can help in lowering the IP beam size. A large effect of the beam orbit on the IP beam size is observed in ATF2. Therefore, improving the existing orbit control in ATF2

might be of crucial importance for the future ultralow β_y^* study.

ACKNOWLEDGMENTS

Many thanks to the whole ATF2 collaboration for supporting this study.

[1] M. Aicheler, P. Burrows, M. Draper, T. Garvey, P. Lebrun, K. Peach, N. Phinney, H. Schmickler, D. Schulte, and N. Toge, CERN Technical Report No. CERN-2012-007, 2012.

[2] The international linear collider technical design report, http://www.linearcollider.org/ILC/Publications/Technical-Design-Report.

[3] P. Raimondi and A. Seryi, Novel Final Focus Design for Future Linear Colliders, Phys. Rev. Lett. **86**, 3779 (2001).

[4] H. Braun *et al.* (ATF2(KEK) Group Collaboration), CERN Technical Reports No. CERN-AB-2005-035, No. CLIC-Note-636, No. DESY-05-148, No. DESY-2005-148, No. ILC-ASIA-2005-22, No. JAI-2005-002, No. KEK-REPORT-2005-2, No. SLAC-R-771, and No. UT-ICEPP-2005-02, 2005.

[5] G. R. White *et al.* (ATF2 Collaboration), Experimental Validation of a Novel Compact Focusing Scheme for Future Energy-Frontier Linear Lepton Colliders, Phys. Rev. Lett. **112**, 034802 (2014).

[6] K. Kubo, Towards an International Linear Collider: Experiments at ATF2, in *Proceedings of the 5th International Particle Accelerator Conference, Dresden, 2014*, p. WEZA01.

[7] S. Kuroda, ATF2 for final focus test beam for future linear colliders, *37th International Conference on High Energy Physics, Valencia, 2014*.

[8] T. Okugi, Small beam status, *European Linear Collider Workshop, Santander, 2016*.

[9] D. Angal-Kalinin *et al.*, Exploring ultralow β^* values in ATF2—R&D program proposal, Technical Report, 2008.

[10] R. Tomas *et al.*, in *Proceedings of the 23rd Particle Accelerator Conference, Vancouver, Canada, 2009* (IEEE, Piscataway, NJ, 2009), WE6PFP024.

[11] E. Marin, R. Tomás, P. Bambade, K. Kubo, T. Okugi, T. Tauchi, N. Terunuma, J. Urakawa, A. Seryi, G. R. White, and M. Woodley, Design and high order optimization of the accelerator test facility lattices, Phys. Rev. ST Accel. Beams **17**, 021002 (2014).

[12] M. Patecki and R. Tomás, Effects of quadrupole fringe fields in final focus systems for linear colliders, Phys. Rev. ST Accel. Beams **17**, 101002 (2014).

[13] M. Masuzawa, Qea magnet measurements at kek and comparison with ihep results, *11th ATF2 Project Meeting, Menlo Park, 2011*.

[14] S. Bai, P. Bambade, D. Wang, J. Gao, M. Woodley, and M. Masuzawa, Mitigating the effects of higher order multipole fields in the magnets of the Accelerator Test Facility 2 at KEK, Chin. Phys. C **36**, 756 (2012).

[15] F. Schmidt, E. Forest, and E. McIntosh, CERN Technical Report No. CERN-SL-2002-044-AP, 2002.

[16] R. Tomás, CERN Technical Report No. AB-Note-2006-017, 2007.

[17] R. Tomás, Nonlinear optimization of beam lines, Phys. Rev. ST Accel. Beams **9**, 081001 (2006).

[18] R. Baartman, Intrinsic third order aberrations in electrostatic and magnetic quadrupoles, in *Proceedings of the Particle Accelerator Conference, Vancouver, BC, Canada, 1997* (IEEE, New York, 1997), p. 4V023.

[19] G. H. Hoffstätter and M. Berz, Symplectic scaling of transfer maps including fringe fields, Phys. Rev. E **54**, 5664 (1996).

[20] E. Marin, SLAC Technical Report No. SLAC-TN-14-019, 2014.

[21] M. Modena, Update on 2 octupoles procurement for atf2 final focus systems, *18th ATF2 Project Meeting, Annecy-le-Vieux, France, 2015*.

[22] S. Bai, A. Aryshev, P. Bambade, D. McCormick, B. Bolzon, J. Gao, T. Tauchi, and F. Zhou, First beam waist measurements in the final focus beam line at the kek accelerator test facility, Phys. Rev. ST Accel. Beams **13**, 092804 (2010).

[23] H. Sakai, M. Fujisawa, K. Iida, I. Ito, H. Kudo, N. Nakamura, K. Shinoe, T. Tanaka, H. Hayano, M. Kuriki, and T. Muto, Improvement of fresnel zone plate beam-profile monitor and application to ultralow emittance beam profile measurements, Phys. Rev. ST Accel. Beams **10**, 042801 (2007).

[24] J. Alabau-Gonzalvo *et al.*, The ATF2 multi-otr system: Studies and design improvements, in *Internation Beam Instrumentation Conference, Tsukuba, 2012*.

[25] M. A. Pons *et al.*, Technical Report No. SLAC-PUB-14684.

[26] T. Shintake, H. Hayano, A. Hayakawa, Y. Ozaki, M. Ohashi, K. Yasuda, D. Waltz, S. Wagner, and D. Burke, Design of laser-Compton spot size monitor, in 15th International Conference on High-Energy Accelerators, Hamburg, 1992, pp. 215–218.

[27] J. Yan, Ph.D. thesis, University of Tokyo, 2015.

[28] T. Okugi, S. Araki, P. Bambade, K. Kubo, S. Kurado, M. Masuzawa, E. Marin, T. Naito, T. Tauchi, N. Terunuma, R. Tomas, J. Urakawa, G. White, and M. Woodley, Linear and second order optics corrections for the kek accelerator test facility final focus beam line, Phys. Rev. ST Accel. Beams **17**, 023501 (2014).

[29] H. Grote and F. Schmidt, CERN Technical Report No. CERN-AB-2003-024-ABP, 2003.

[30] T. Okugi, IP beam size tuning in these 2 weeks, at the ATF2 operation meeting, 2016.

[31] M. Patecki, Summary of low β^* experiment in this week, at the ATF2 Operation Meeting, 2016.